ELSEVIER

Chemical Geology 225 (2006) 347–359

CHEMICAL GEOLOGY
INCLUDING
ISOTOPE GEOSCIENCE

www.elsevier.com/locate/chemgeo

Distinct local environments for Ca along the non-ideal pyrope–grossular solid solution: A new model based on crystallographic and EXAFS analysis

Roberta Oberti [a,*], Simona Quartieri [b], Maria Chiara Dalconi [b,1], Federico Boscherini [c], Gianluca Iezzi [d], Massimo Boiocchi [e]

[a] *CNR, Istituto di Geoscienze e Georisorse, sezione di Pavia, via Ferrata 1, I-27100 Pavia, Italy*
[b] *Dipartimento di Scienze della Terra, Università di Messina, Salita Sperone 31, I-98166 Messina S. Agata, Italy*
[c] *Dipartimento di Fisica and INFM, Università di Bologna, Viale Berti Pichat 6/2, I-40127 Bologna, Italy*
[d] *Diartimento di Scienze della Terra, Università di Chieti, via dei Vestini 30, I-66013 Chieti Scalo, Italy*
[e] *Centro Grandi Strumenti, Università di Pavia, via Bassi 21, I-27100 Pavia, Italy*

Accepted 16 August 2005

Abstract

A multi-technique approach (based on electron microprobe analysis, structure refinement, and EXAFS analysis at the Ca K-edge) was used to characterise the local geometry of Ca in synthetic and natural garnet compositions referable to the pyrope–grossular solid solution. Multi-shell fits of the EXAFS data indicate that Ca assumes the standard [4+4]-fold coordination (the polyhedral shape being a triangular dodecahedron with Ca1–O=2.30–2.31(1) and Ca2–O=2.45–2.46(1) Å) when Ca>1.50 atoms per formula unit (apfu), but assumes a nearly regular [8]-fold coordination with Ca–O=2.35–2.36 (1) Å when (Mg, Fe^{2+}, Mn^{2+})>1.50 apfu. Therefore, in the pyrope-dominant structure the Ca1–O distance lengthens and the Ca2–O distance shortens to converge towards the value observed for the Mg2–O bond in pyrope. This finding is consistent with many distinct structural features observed in solid solution terms with (Mg, Fe^{2+}, Mn^{2+})>1.50 apfu or Ca>1.50 apfu, as well as with the anomalous properties of the intermediate terms observed both in the short-range and in the long-range perspective. The presence of two distinct Ca coordinations in the pyrope (almandine, spessartine)-like and in the grossular-like structure, and thus of an isosymmetric transition at the intermediate composition, can help to explain both the strong and asymmetric non-ideality of the solid solution between pyrope (almandine) and grossular, as well as the differences in the ability to incorporate some trace elements (such as REE and actinides) which are commonly used as process-specific indicators. This feature must be taken into account when building theoretical models of the garnet solid solutions, which are at the moment the most promising approach for calculating thermodynamic properties or for interpreting and predicting trace-element behaviour in this crucial mineral phase.

Keywords: Calcium; Local coordination; Garnets; EXAFS; XANES; Trace-element incorporation

1. Previous work

Garnets are a group of minerals of primary importance for Earth Sciences. They are among the phases most investigated in order to obtain process-specific

* Corresponding author. Tel.: +39 0382 985885; fax: +39 0382 985887.
E-mail address: oberti@crystal.unipv.it (R. Oberti).
[1] Present address: Dipartimento di Scienze della Terra, Università di Ferrara, via Saragat 1, I-44100 Ferrara, Italy.

0009-2541/$ - see front matter © 2005 Elsevier B.V. All rights reserved.
doi:10.1016/j.chemgeo.2005.08.027

information. Their composition and crystal-chemistry is used in geothermobarometers and geospeedometers, and their capacity for incorporating trace elements is exploited to unravel melting and crystallisation processes. Moreover, synthetic compounds with the garnet structure have important properties of industrial and technological application (e.g., the laser technology).

The structure, crystal-chemistry and thermodynamic properties of the various garnet compositions have been extensively studied by many techniques, each one of which has helped to clarify different features at different length scale. Of particular interest for Earth Sciences is the study of the solid solutions between the end-members: pyrope (prp, $Mg_3Al_2Si_3O_{12}$), almandine (alm, $Fe_3^{2+}Al_2Si_3O_{12}$), spessartine (sps, $Mn_3^{2+}Al_2Si_3O_{12}$), grossular (grs, $Ca_3Al_2Si_3O_{12}$) and andradite (adr, $Ca_3Fe_2^{3+}Si_3O_{12}$). The most important aspects that have not yet been completely clarified are related to the strong non-ideality of the solid solutions pyrope–grossular and almandine–grossular. From the structure viewpoint, non-ideality can be evidenced both at the long-range scale (e.g., Merli et al., 1995; Ungaretti et al., 1995) and at the short-range scale (cf. the recent exhaustive review by Geiger, 2004). It is also evidenced in thermodynamic properties (e.g., Ganguly et al., 1993; Bosenick et al., 2000, 2001; Vinograd et al., 2004) and trace-element incorporation (van Westrenen et al., 1999). The strongest deviations from ideal behaviour are always observed around the 50:50 compositions. There is a general consensus in relating this situation to the substitution of a large cation ($^{[8]}Ca = 1.12$ Å) by a small cation ($^{[8]}Mg = 0.89$, $^{[8]}Fe^{2+} = 0.92$, and $^{[8]}Mn^{2+} = 0.96$ Å) at the dodecahedral X site (Fig. 1), to the consequent structural strain, and to the mechanisms and length scale of local relaxation. The presence of local heterogeneity at the unit-cell scale is presently assumed to provoke the observed anomalies.

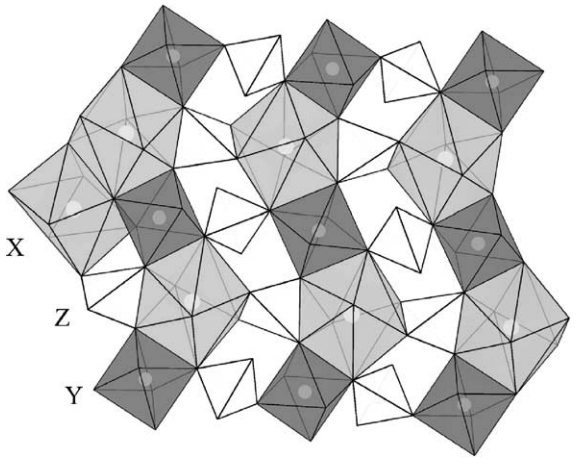

Fig. 1. A sketch of the garnet structure, showing the extensive edge-sharing between the different polyhedra.

Details of the various approaches used to clarify the relevant aspects are provided in the discussion of the results of this work. Here it is important to recall that several models have been proposed to simulate the substitution of Ca by (Mg, Fe^{2+}, Mn^{2+}), but none was found to explain all the experimental observations. Among them: (i) the linear mixing of constant local environment for large and small cations (i.e., a model of alternating bonds, with complete local relaxation); (ii) the use of hybrid sites with sizes and bonding properties calculated as weighted averages of those of the components (virtual crystal approximation with no local relaxation); (iii) the hypothesis that the local environment of the small cation (especially Mg) may expand as a function of the Ca content in the structure. Static lattice energy calculations and atomistic simulations of the prp–grs solid solution were also attempted both to calculate thermodynamic properties of mixing (Bosenick et al., 2001; Vinograd et al., 2004) and to model trace-element incorporation and solution energies (van Westrenen et al., 2003a,b; Allan et al., 2003). Bosenick et al. (2001) found that simulations made with model (i) reproduce the extent of the anomalies in ΔV_{mix} and related thermodynamic properties, but cannot reproduce their asymmetry. On the contrary, a simulation done with model (ii) yields parameters that are several factors larger than the experimental ones. van Westrenen at al. (2003a,b) compared their results with experimental trace-partitioning data and concluded that the use of the virtual crystal approximation is inadequate. The use of discrete and constant Mg and Ca sites reproduces the anomalously high solubility of trace elements observed around $prp_{50}grs_{50}$, but in terms of local order implies violation of the Goldschmidt's first rule because large trace elements may substitute for Mg and small trace elements for Ca.

Allan et al. (2003) reviewed the available data on atomistic simulations of mineral solid solutions, and concluded that "it is crucial to take explicit account of the local structural environment of each ion"... "and of its changes following the introduction of a foreign atom". It is therefore important to obtain reliable information on the local configuration of Ca and on its possible variation along the garnet solid solutions of interest.

In the latest few years, we have undertaken a systematic multi-technique study of garnet solid solutions, which includes X-ray absorption spectroscopy (XAS, Lee et al., 1981; Koninsberger and Prins, 1988). XAS is

an element-specific technique particularly useful in describing local structural and dynamical properties (site symmetry, interatomic distances, type and number of neighbouring atoms, and Debye–Waller factors) for major, minor and trace elements. Hence, XAS is well suited to study the local structural environment around a specific cation involved in a solid solution; it has been successfully applied to investigate the local environment of REE in both synthetic and natural garnets (Quartieri et al., 1999a,b, 2002, 2004a) and to study the bonding and vibrational properties of the X cations in natural garnets and synthetic almandine–spessartine solid solutions (Quartieri et al., 1993, 1997; Sani et al., 2004).

The specific problem of the local environment of Ca in garnet solid solutions was first addressed by Quartieri et al. (1995), who discussed XANES analysis at the Ca K-edge of selected natural samples which had been already characterised by electron microprobe analysis and single-crystal structure refinement. These authors concluded that: (i) the changes in the XANES spectra observed as a function of Ca content are essentially due to the local geometry of the absorbing atom, which undergoes a deformation as a consequence of the Mg, Fe substitution; (ii) such deformation of the Ca coordination is not linear along the join.

This work reports new XANES and EXAFS data analysis, and provides quantitative information on the local coordination of Ca in a suite of natural and synthetic garnets selected to cover the prp–grs join and to analyse the possible effects of the entrance of other cations at the various structural sites (e.g., Fe^{2+} and Sc at the X site, Fe^{3+} and Sc at the Y site, H and Sc at the Z site).

2. Sample material and analytical methods

The main object of this work is to detect and monitor the changes in Ca coordination along the join pyrope–grossular. Because the size and distortion of the X dodecahedron has been shown to depend strongly on the site populations of all the structural sites (cf. Merli et al., 1995; Ungaretti et al., 1995 for a review of garnet crystal-chemistry and structural modifications), we used both synthetic samples with simple compositions and natural samples with more complex compositions. A short description of the samples is given in Table 1.

2.1. Synthesis

The synthetic garnets used in this work were designed for a complementary study (still in progress) on Sc incorporation in the pyrope–grossular join (Quartieri et al., 2004b,c). Therefore, the starting material was prepared by mixing oxides and carbonates in the appropriate percentages (prp_{100}, $prp_{60}grs_{40}$, $prp_{20}grs_{80}$ and grs_{100}) with the addition of 5 wt.% of Sc_2O_3 (99.9%). All the synthesis experiments were done with an end-load 0.5-in. piston cylinder apparatus at the Bayerisches Geoinstitut, using the classical *hot piston-in* technique and working at 1000 °C and 3 GPa for 24 h. To improve garnet homogeneity, the run-products were powdered and reannealed for 24 h at 1100 °C and 4 GPa after adding about 25 wt.% of the starting mixtures of oxides and 2 wt.% water. This procedure was found to be successful by Ganguly et al. (1993); however, these authors could work at 1400 °C, a T value that could not be approached in the experiments of this work. The run products were controlled and characterised by electron microprobe analysis, X-ray powder diffraction and (when allowed by crystal size) single-crystal structure refinement. The run products are composed only of garnets, although with sample inhomogeneity, especially in the intermediate composition (Table 1). All the runs produced well formed crystals with equant habit. Their crystal size is strongly dependent on composition: Sc-doped pyrope may reach 1 mm, Sc-doped grossular rarely exceeds 50 μm, and crystals with the intermediate compositions are typically between 5 and 20 μm. Details of the prepara-

Table 1
Sample codes, unit formulae (based on 12 oxygen atoms) and references for the samples used in the present study

No.	Code	Unit formulae	Reference
1	Sc-doped Grs	$(Ca_{2.86}Sc_{0.14})(Al_{1.83}Sc_{0.17})(Si_{2.86}Sc_{0.14})O_{12}$*–$(Ca_{2.89}Sc_{0.11})(Al_{1.85}Sc_{0.15})(Si_{2.89}Sc_{0.11})O_{12}$	This work
2	Sc-doped $Prp_{20}Grs_{80}$	$(Ca_{2.32}Mg_{0.48}Sc_{0.20})(Al_{1.86}Sc_{0.14})(Si_{2.80}Sc_{0.20})O_{12}$–$(Mg_{0.63}Ca_{2.31}Sc_{0.06})(Al_{1.80}Sc_{0.20})(Si_{2.94}Sc_{0.06})O_{12}$	This work
3	Sc-doped $Prp_{60}Grs_{40}$	$(Ca_{1.20}Mg_{1.65}Sc_{0.15})(Al_{1.82}Sc_{0.18})(Si_{2.85}Sc_{0.15})O_{12}$–$(Mg_{2.02}Ca_{0.98})(Al_{1.85}Sc_{0.15})(Si_{3.00})O_{12}$	This work
4	MP12	$(Ca_{0.51}Mg_{0.91}Fe^{2+}_{1.54}Mn_{0.04})(Al_{1.98}Fe^{3+}_{0.02})Si_{3.0}O_{12}$	Quartieri et al., 1995
5	BRIC	$(Ca_{2.89}Fe^{2+}_{0.07}Mn_{0.04})(Al_{1.00}Fe^{3+}_{0.76}Fe^{2+}_{0.12}Ti^{4+}_{0.12})(Si_{2.93}H_{0.28})O_{12}$	Quartieri et al., 1995

The synthetic Sc-doped garnets are inhomogeneous: * denotes the composition most coherent with single-crystal structure refinement.

tion of the starting materials, synthesis and characterisation of Sc site-preference are reported elsewhere (Quartieri et al., 2004b,c and manuscript in preparation). The final formulae of the products, obtained by combining electron microprobe and EXAFS analysis with structure refinement, are listed in Table 1. In all the garnets used in the present study, Sc partitions itself among the X, Y and Z sites; however, the nearly constant occupancies at the various sites observed along the solid solution allow a reliable investigation of the changes in the local environment of Ca as a function of the Mg content.

2.2. Natural samples

Sample 4 (MP12) occurs in metasedimentary rocks of the Ivrea–Verbano Zone (Italy), and was chosen in order to characterise the Ca environment in (Mg, Fe^{2+}, Mn^{2+})-rich compositions, its grossular component being 17%.

Sample 5 (BRIC, from Bric Canizzi, Liguria, Italy; Quartieri et al., 1995) has a complex site population, with Fe^{2+} and Ti^{4+} substituting for Al^{3+} at the Y site, and a significant hydrogrossular component at the Z site. It has been used to check whether and how such substitutions at the Y and Z sites affect the Ca environment in grs-rich compositions.

2.3. Electron microprobe analysis

For the synthetic samples, SEM-EDS analysis was carried out at the Bayerisches Geoinstitut with a Leo-Gemini scanning electron microscope equipped with an Oxford EDAX detector on carbon coated thin sections where some mg of crushed and polished run-products had been mounted. Electron microprobe (EMP) analysis was done using a CAMECA SX-50 in WDS operative mode with the following conditions: 15 kV excitation voltage, 15 nA beam current, 20 s counting time on peak and 10 s counting time on background, with an electron beam smaller than 2 μm. The standards used were: diopside for Ca (PET) and Mg (TAP), albite for Al and Si (TAP), and pure Sc_2O_3 oxide for Sc (PET). Data reduction was done using the PAP method (Pouchou and Pichoir, 1985).

Details of the EMP analyses and unit-formulae calculation of the natural samples are reported in Quartieri et al. (1995).

2.4. X-rays analysis and structure refinement

Single-crystal X-ray data for the natural samples (4 and 5) were collected at the CNR-IGG-PV with a Philips PW1100 diffractometer (monochromatised MoKα radiation) in the 2θ range 4–80°. Details of the data collection and treatment are given in Quartieri et al. (1995).

For the synthetic Sc-doped grossular (crystal size $0.03 \times 0.03 \times 0.015$ mm), X-ray diffraction data were collected at the CNR-IGG-PV with a Bruker-AXS Smart-Apex CCD-based diffractometer, working with graphite monochromatised MoKα radiation at 55 kV and 30 mA. Omega rotation frames (scan width 0.2°, scan time 90 s, sample-to-detector distance 4 cm) were collected using the SMART software (© Bruker-AXS Inc.). Data reduction (including intensity integration, background, Lorentz and polarisation corrections) was done with the SAINT software (© Bruker-AXS Inc.). Absorption effects were evaluated analytically by the SADABS software (Sheldrick, 1996), and the data were corrected accordingly. The length of the unit-cell edge was obtained from least-squares refinements of the center of gravity of 2108 independent reflections in the 2θ-range 12–80°.

For all the three samples, structure refinement (SREF) was done with a program locally developed to deal with a complex solid solution (Cannillo, personal communication) using scattering factors for fully ionised chemical species. Reflections with $I > 3\sigma(I)$ were considered as observed during unweighted full-matrix least-squares refinements on F.

X-ray powder diffraction (XRPD) patterns were recorded in the 2θ range 8–100° (CuKα_1–α_2 radiation), with a step scan of 0.02° and a counting time of 10 s per step using a Siemens D5000 diffractometer operating in Bragg–Brentano geometry at the Bayerisches Geoinstitut. The diffraction patterns were refined with the Rietveld whole-pattern method using the EXPGUI-GSAS software package (Toby, 2001; Larson and Von Dreele, 1997). The values of the unit-cell edge and of the coordinates of the oxygen atom were refined starting from the SREF values of Sc-doped pyrope and grossular single crystals. The site occupancies were fixed to those obtained by the SREF data for Sc-doped grossular, and to those derived from EMP data for the intermediate garnet compositions.

The final refinement parameters and bond distances for all the samples are reported in Table 2. Both the single-crystal and powder data are reported for grossular to show the level of consistency between the two methods and to take into account the chemical variability (Table 1), which is not covered by the single-crystal data. Notably, chemical inhomogeneity causes a broadening on the diffraction peaks, and thus a lowering of the quality of the Rietveld refinement.

Table 2
Selected results of the structure refinements of the samples used in the present study

No.	a (Å)	R_{all} %	X1–O (Å)	X2–O (Å)	<X–O> (Å)	Y–O (Å)	Z–O (Å)	Sh X–X (Å)	Unsh X (Å)	Sh X–Y (Å)	Unsh Y (Å)
1	11.883(1)	6.0	2.326(1)	2.488(1)	2.407(1)	1.939(1)	1.650(1)	2.961(1)	2.864(1)	2.771(1)	2.714(1)
1*	11.891(1)	7.0	2.331(1)	2.473(1)	2.402(1)	1.954(1)	1.650(1)	2.935(1)	2.838(1)	2.786(1)	2.741(1)
2*	11.820(1)	5.0	2.308(1)	2.457(1)	2.382(1)	1.927(1)	1.658(1)	2.916(1)	2.844(1)	2.734(1)	2.715(1)
3*	11.649(1)	7.0	2.243(1)	2.397(1)	2.320(1)	1.915(1)	1.650(1)	2.788(1)	2.820(1)	2.677(1)	2.740(1)
4	11.571(1)	2.6	2.231(1)	2.390(1)	2.310(1)	1.897(1)	1.636(1)	2.790(1)	2.814(1)	2.659(1)	2.705(1)
5	11.967(1)	2.7	2.344(1)	2.497(1)	2.421(1)	1.973(1)	1.650(1)	2.958(1)	2.863(1)	2.819(1)	2.762(1)

* Rietveld refinement on X-ray powder-diffraction data; $R_{SC}=R_F=\Sigma|F_{obs}-F_{calc}|/\Sigma F_{obs}$; $R_{Riet}=R_F^2=\Sigma|F_{obs}^2-F_{calc}^2|/\Sigma F_{obs}^2$.

2.5. XAS measurements

Samples were prepared by grinding the garnet powders in a mortar to reduce the grain size, mixing them with cellulose and finally pressing them into 2 mm diameter pellets. Data were collected at the beamline ID26 of the European Synchrotron Radiation Facility. ID26 is a high-brilliance insertion-device source equipped with two mirrors for beam focalisation and harmonic rejection and a double-crystal monochromator (two flat Si(111) crystals in our experiment). XANES and EXAFS Ca K-edge spectra were measured in the fluorescence mode using photo-diode detectors. Data acquisition was done in the quick scan mode, consisting in a synchronous movement of the undulator gap and the Bragg angle of the monochromator. Several scans were averaged for each sample.

2.6. XAS data analysis

XANES spectra were analysed according to standard procedures. The raw XANES spectra were subtracted of the pre-edge background and then normalised on the high-energy side. This normalisation procedure takes care of effects resulting from different sample thicknesses, and allows comparison of samples with different absorber contents. The EXAFS signals were extracted from the experimental absorption spectra and analysed using the interactive program IFEFFIT (Newville, 2001) with the support of the graphical utilities ATHENA and ARTEMIS (http://feff.phys.washington.edu/~ravel/software/exafs/). The theoretical XAFS signals were calculated using the FEFF8 code (Ankudinov et al., 1998) based on the garnet structure as determined by structure refinement (from X-ray single-crystal or powder-diffraction data). For all the spectra, a background (bkg) spline was chosen with the number of knots determined by the energy range of the data and by the R_{bkg} parameter set equal to 1.0 Å. The Fourier transform parameters used in the analysis were the following: R-range = 1.2–3.3 Å and k-range = 2.3–10 $Å^{-1}$ for samples 1 and 2; R-range = 1.0–2.7 Å and k-range = 2.3–9.5 $Å^{-1}$ for samples 3 and 4; R-range = 1.1–3.4 Å and k-range = 2.3–11 $Å^{-1}$ for sample 5. A Hanning window with apodization of 1.0 $Å^{-1}$ was used in each Fourier transform. The adjustable parameters optimised in the fitting procedure were: an energy shift equal for all paths (ΔE_0), a change in the path length (ΔR_i) and the relative mean-square displacement of atoms (σ_i^2). The numbers of identical paths (N_{degen}) were kept fixed according to the structural models. The passive electron reduction factor (S_0^2) was obtained by fitting the Ca K-edge data from the reference compound with known structure (CaO). Data from CaO, measured in fluorescence mode, were corrected for self-absorption effects (Carboni et al., 2005). The value for $S_0^2=0.6$ was determined.

3. Results

3.1. XANES results

The XANES spectra of the samples of this study are reported in Fig. 2. Spectra are ordered from top to bottom as a function of the Ca content. Several features are clearly resolved in all the spectra, and are labelled from A to H moving towards higher energy. The intensities of some features strongly vary with the Ca content, suggesting changes in the local environment of Ca along the series. All spectra are characterised by a small pre-edge (feature A), whose energy and intensity is independent of the Ca content. At higher energy, a strong three-peaked resonance is found, corresponding to the main $1s \rightarrow np$ transition. The shoulder-like structure (B) at the low-energy side remains unchanged throughout the series, whereas the intensity ratio of the two most prominent peaks (C and D) strongly depends on the Ca content. In particular, the intensity of feature D is inversely related to the grossular component. At higher energy, further structures are almost constant throughout the series with the exception of

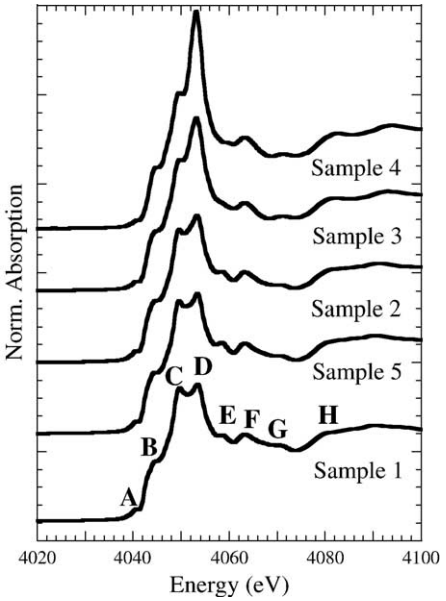

Fig. 2. XANES spectra at the Ca K-edge. Individual spectra have been normalized with respect to the high-energy side of the curve.

feature E, which is extremely weak, or almost absent, in the low-Ca samples.

These findings confirm and extend the conclusions drawn by Quartieri et al. (1995), who examined the Ca K-edge XANES spectral features of a series of natural garnets, and concluded that Ca in the grossular-poor compositions (pyralspites) is not in the same structural configuration as in the grossular-rich ones. Quartieri et al. (1995) inferred that Ca was likely to adapt its coordination to the geometrical constraints imposed by the dominant cation at the X site.

3.2. EXAFS results

Fig. 3 reports the background subtracted EXAFS spectra of all the samples of this study. The Fourier transforms and the back-Fourier transforms of the EXAFS data, with the fitted signals, are reported in Fig. 4 (left and right columns, respectively).

3.2.1. Sample 1: synthetic Sc-doped grossular

A three-dimensional picture of the structural model used for the simulation of the EXAFS signal is given in Fig. 5. The Ca absorber atoms are surrounded by 4+4 oxygen atoms at two symmetrically independent bond distances (corresponding to X1–O and X2–O), 2 Si atoms corresponding to the second coordination shell, 4 Al atoms at a larger distance corresponding to the third shell, and 4 Si atoms plus 4 Ca atoms at the same distance corresponding to the fourth coordination shell.

The Fourier transform of the spectrum from sample 1 and the fitted signal are reported in Fig. 4a (left). The first two peaks can be related to the contributions of the first oxygen shell (4+4 oxygen atoms at two different distances) and of the second shell (2 Si atoms), respectively. The structure in the region between 2.6 Å and 3.4 Å is the result of the contributions from several atoms in the third and fourth coordination shell, so that the contribution from each path cannot be distinguished straightforwardly. To reduce the total number of fitted parameters, the following constraints were used: one energy shift for all paths (ΔE_0), two σ_i^2 values for the oxygen shells, one common σ_i^2 value for Si and Al paths and one distinct σ_i^2 value for Ca path, five independent path length (ΔR_i) values. The Si and Ca atoms at the same distance in the fourth shell were constrained to have the same ΔR_i value. Table 3 and Fig. 4a (right) report the fitting results.

3.2.2. Sample 5: BRIC

The gross features of the Fourier transforms of the $|\chi(R)|$ data for the synthetic Sc-doped grossular and for BRIC (Fig. 4a and b) are similar, with the exception of the peak at 3 Å (not phase corrected), which shows a remarkable decrease in amplitude in the latter sample. Because the X-site population is virtually the same in the two samples, the observed intensity variation must be related to the population of the crystallographic Y site ($Al_{1.83}$ and $Sc_{0.17}$ in Sample 1 and $Al_{1.00}Fe^{3+}_{0.76}Fe^{2+}_{0.12}Ti^{4+}_{0.12}$ in sample 5). To account for the presence of two dominant cations (Al and Fe^{3+}) at the octahedral site of sample 5, distinct Ca–Al and Ca–Fe paths were used in the fitting procedure, with independent ΔR_i parameters, and multiplicities based on the sample stoichiometry. Best-fit results are reported in Table 4 and in Fig. 4b (right). To reduce the number of total fitted parameters, the fourth-shell Ca–Si and Ca–Ca

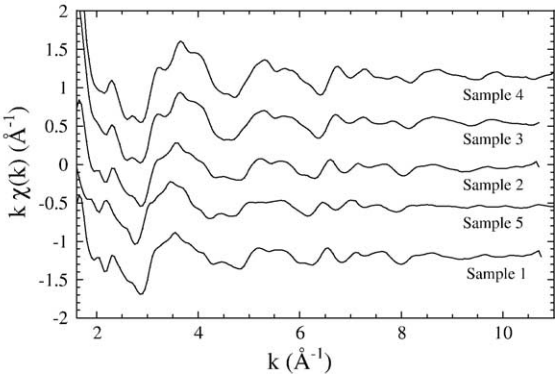

Fig. 3. Background subtracted Ca K-edge EXAFS spectra. The spectra of samples 2–5 have been translated vertically to improve clarity.

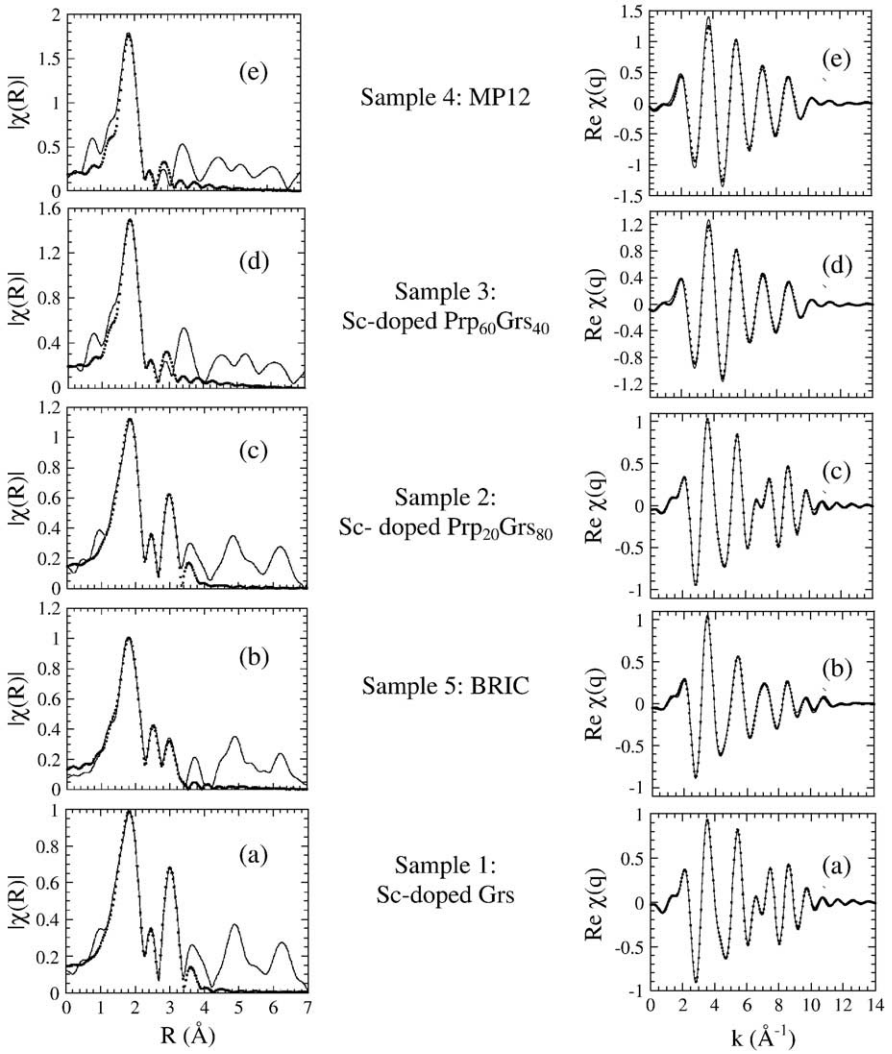

Fig. 4. Left panels: Fourier transforms of the Ca K-edge data (solid line) and fitted signals (dots). Right panels: the anti-Fourier transforms of the EXAFS data (solid line) and the fitted signals (dots).

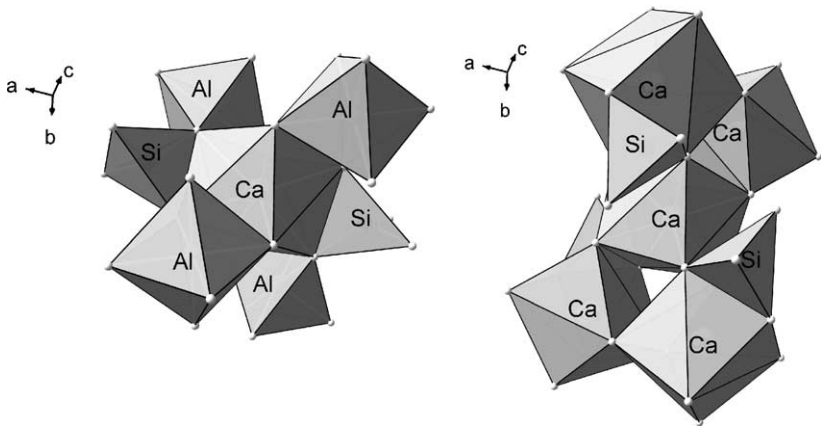

Fig. 5. Local average environment of Ca absorber atom in the dodecahedral site (X) of the garnet structure. For clarity, only the second and third coordination shells are represented on the left sketch, whereas only the fourth shell is represented on the right.

Table 3
Sample 1: fit results for the Ca K-edge data

Distance	N_{degen}	R (Å)	σ_i^2 (Å^2)	<SREF> (Å)
Ca–O	4	2.31(1)	0.003(1)	2.326(1)
Ca–O	4	2.46(1)	0.004(1)	2.488(1)
Ca–Si	2	2.98(1)	0.004(1)	2.971(1)
Ca–Al	4	3.34(1)	0.004(1)	3.321(1)
Ca–Si	4	3.65(1)	0.004(1)	3.638(1)
Ca–Ca	4	3.65(1)	0.007(2)	3.638(1)
Ca–O	4	3.68(1)	0.004(1)	3.705(1)

S_0^2 =0.6; $\Delta E_0 = 7 \pm 1$; R-factor=0.0012.

paths were constrained to have the same ΔR_i and σ_i^2 parameters.

It is noteworthy that the high quality of the EXAFS signal and of the data analysis, which could be performed up to the fourth shell around the absorber atoms, allows us to distinguish two different interatomic distances between Ca and the major octahedral cations (Fe^{3+} and Al) in this sample (see Table 4). Interestingly, the mean Ca–Y distance obtained by single-crystal structure refinement is in good agreement with that derivable by averaging the results of the EXAFS analysis.

3.2.3. Sample 2: synthetic Sc-doped $Prp_{20}Grs_{80}$

The same model and constraints described in Section 3.2.1 were applied to fit the data from sample 2. The fit results are reported in Table 5 and Fig. 4c. The Fourier transforms of samples 1 and 2 are closely related (Fig. 4a, c), indicating that the local environment of the Ca atoms in this compositional range is not affected by the presence of the prp component. The small changes in the amplitudes of the first and third peak are reflected in the changes of the fitted σ_i^2 values for the first oxygen shell and the Ca–Ca path (cf. Tables 3 and 5).

3.2.4. Sample 3: synthetic Sc-doped $Prp_{60}Grs_{40}$

The remarkable differences in peak positions and amplitudes between the $|\chi(R)|$ data sets shown in Fig. 4 (a–c, left, and d–e, left) indicate a strong change in the local environment of the Ca atoms. Therefore, the structural model and the multi-shell fitting procedure used in the data analyses of the previous samples can no longer be applied to these samples. Notably, sample 3 is rather inhomogeneous, but all the crystal-chemical formulae obtained by EMP analysis show that the small cations (Mg+Sc) dominate over Ca. Best fit results of the first peak of the Fourier transform indicate that the two first-shell oxygen paths with multiplicity 4 tend to assume about the same distance from the Ca absorber atoms. The space resolution obtainable by our EXAFS data did not allow an independent fit of the two paths. Hence, the first coordination shell of Ca was fit with a unique oxygen path with multiplicity 8. Best-fit results of the first two shells are reported in Table 6 and Fig. 4d (right). A fit extended to the third shell, similar to those discussed above, could not be obtained for this sample, probably due to the large structural disorder and the imperfect match between our model and the real structure.

Table 4
Sample 5: fit results for the Ca K-edge data

Distance	N_{degen}	R (Å)	σ_i^2 (Å^2)	<SREF> (Å)
Ca–O	4	2.33(1)	0.003(1)	2.344(1)
Ca–O	4	2.48(1)	0.003(2)	2.497(1)
Ca–Si	2	3.01(1)	0.002(3)	2.992(1)
Ca–Fe	4*0.5	3.41(2)	0.008(10)	3.345(1)
Ca–Al	4*0.5	3.33(3)	0.003(1)	
Ca–Si	4	3.69(1)	0.005(6)	3.665(1)
Ca–Ca	4	3.69(1)	0.005(6)	3.665(1)

S_0^2 =0.6; $\Delta E_0 = 6 \pm 1$; R-factor=0.007.

Table 5
Sample 2: fit results for the Ca K-edge data

Distance	N_{degen}	R (Å)	σ_i^2 (Å^2)	<SREF> (Å)
Ca–O	4	2.30(1)	0.001(1)	2.308(1)
Ca–O	4	2.45(1)	0.002(1)	2.457(1)
Ca–Si	2	2.98(1)	0.003(1)	2.955(1)
Ca–Al	4	3.33(1)	0.003(1)	3.304(1)
Ca–Si	4	3.64(1)	0.003(1)	3.619(1)
Ca–Ca	4	3.64(1)	0.014(3)	3.619(1)
Ca–O	4	3.67(1)	0.004(1)	3.701(1)

S_0^2 =0.6; $\Delta E_0 = 7 \pm 1$; R-factor=0.0027.

3.2.5. Sample 4: MP12

As shown in Fig. 4e (left), the Fourier transform of sample 4 closely resembles that of sample 3. Hence, the EXAFS data were fitted based on the same fitting procedure used for sample 3, and the results are shown in Table 7 and Fig. 4e (right).

3.3. Combining EMP, EXAFS and structure refinement results

The structural variations most relevant in the present context are shown in Fig. 6, where the results of the present work are compared to the trends obtained from

Table 6
Sample 3: fit results for the Ca K-edge data

Distance	N_{degen}	R (Å)	σ_i^2 (Å^2)	<SREF> (Å)
Ca–O	8	2.36(1)	0.004(1)	2.320(1)
Ca–Si	2	2.92(2)	0.012(9)	2.912(1)

S_0^2 =0.6; $\Delta E_0 = 8 \pm 2$; R-factor=0.007.

Table 7
Sample 4: fit results for the Ca K-edge data

Distance	N_{degen}	R (Å)	σ_i^2 (Å^2)	<SREF> (Å)
Ca–O	8	2.35(1)	0.002(1)	2.310(1)
Ca–Si	2	2.86(2)	0.013(17)	2.893(1)

S_0^2 =0.6; $\Delta E_0 = 8 \pm 3$; R-factor=0.010.

single-crystal refinements done on garnets at the CNR-IGG-PV. In the garnet structure, a change in the site population of a given site affects the size and the distortion of all the other sites (and hence the length of the unit-cell edge). The strong interdependence of the geometry of the various structural sites derives from the extensive edge sharing between the various polyhedra (Fig. 1). For instance, the occurrence of cations larger than Al (namely, Fe^{3+}, Sc, Ti and Fe^{2+}) at the Y site not only strongly affects the size and the geometry of the Y octahedron (Fig. 6c), but also the geometry of the X dodecahedron, whose site population is fixed to pure Ca in the grs–adr join (Fig. 6 a and b). Therefore, any speculation based on bond distances in a given garnet composition should be verified by comparison with the expected trend obtained from a representative database.

Merli et al. (1995) showed that the most effective way to model structural variations in garnet solid solutions is to plot the parameters of relevance as a function of the unit-cell edge. In this way, simple paths of structural variations are identified, and the effects of the chemical exchanges can be evaluated based on the position of the relevant end-members. For example: (i) the position of sample 4 (a=11.571 Å) in Fig. 6a–c is consistent with a mixture of 52% alm, 31% prp and 17% grs, and with the absence of large cations at the Y site; (ii) the positions of samples 1 and 2 (a=11.883 and 11.820 Å, respectively) are consistent with their X-site populations (95% grs 5% prp (+Sc) and 80% grs 20% prp, respectively; based on the similarity of their ionic radii, 0.87 vs. 0.89 Å, $^{[8]}$Sc can be summed to $^{[8]}$Mg) and with the presence of a large cation at the Y site (in their case, Sc).

Fig. 6 shows that, for a long-range perspective (averaged over the investigated crystal), the anomalies in the (prp, alm, sps)–grs solid solution are only slightly apparent in the behaviour of the X1–O and X2–O distances, and cancel out in the <X–O> distance, which increases almost linearly (Fig. 6a). On the other hand, inspection of the values assumed by the shared and unshared edges at the X and Y polyhedra (Fig. 6 b and c, respectively) shows distinct coordination geometries in the two distinct regions with Ca<1.50 and Ca>1.50 apfu. Further and even stronger structural anomalies are observed at intermediate compositions for the various long-range indices of polyhedral distortion; they are surely related to the need for local relaxation via polyhedral distortion, but cannot be discussed in the context of this work. Notably, garnet compositions with Ca slightly exceeding 1.50 apfu cannot be found in nature (and those close to (prp, alm, sps)$_{50}$grs$_{50}$ are always enriched in alm), suggesting

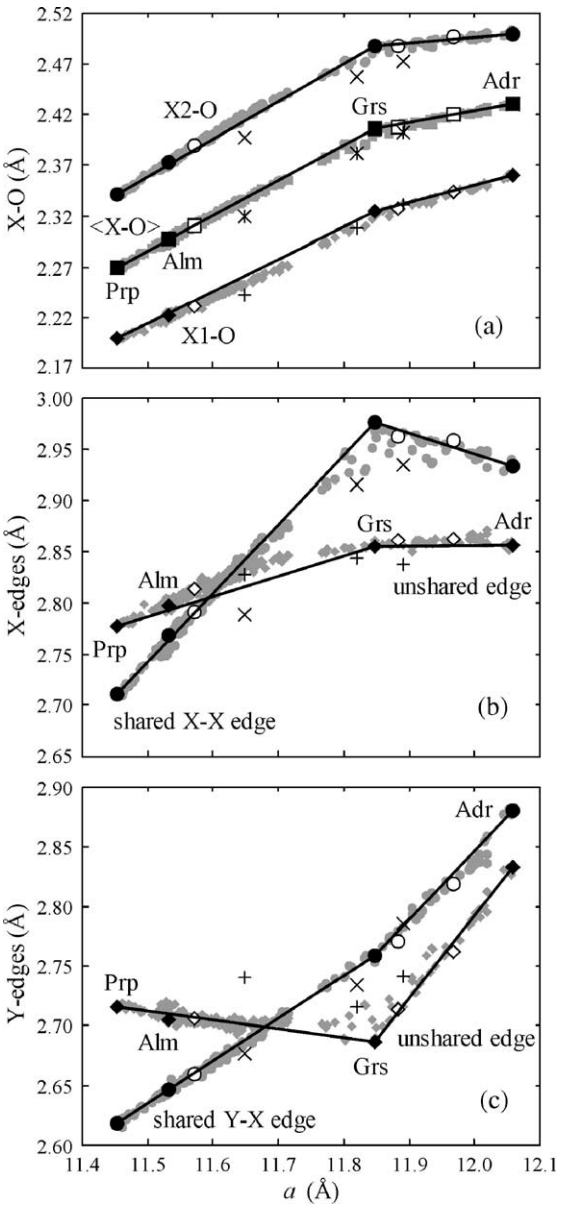

Fig. 6. A long-range description of the structural changes along the prp–grs and grs–adr joins from single-crystal refinements in the IGG-CNR-PV database. Filled symbols=end members; grey symbols=solid solutions; empty symbols=single-crystal refinements and crosses=Rietveld refinements for the samples of this work; solid lines represent ideal mixing behaviour.

a structural instability in the range of *a* values between 11.71 and 11.77 Å (Fig. 6), at least at ordinary *P*, *T* conditions. Accordingly, the existence of a miscibility gap below 500 °C has recently been predicted by Vinograd et al. (2004) combining static lattice energy calculations with the chemical-elastic formalism.

The most important conclusion drawn from EXAFS analysis is that the geometry of the local coordination of Ca is not constant along the solid solution. In particular, we can distinguish between two distinct situations: the compositions with Ca > 1.50 apfu and those with $(Mg+Fe^{2+}+Mn^{2+}+Sc) > 1.50$ apfu. The two distinct Ca–O distances obtained for samples 1 (Ca = 2.86 apfu) and 2 (Ca = 2.32 apfu) are identical within the estimated error: 2.31(1) and 2.46(1) Å vs. 2.30(1) and 2.45(1) Å. The two Ca–O distances obtained for sample 5 (Ca = 2.89 apfu) are slightly longer, namely 2.33(1) and 2.48(1) Å. In all these samples, the difference between the two distances (Δ) is always 0.15 Å, and the shape of the coordination polyhedron is a distorted triangular dodecahedron. The Ca–O distances refined for sample 1 (2.326(1) and 2.488(1) Å) are identical to those refined for the end-member grossular synthesised by Ganguly et al. (1993), namely 2.325(1) and 2.488(1) Å, respectively. We can conclude that the site partitioning of Sc between three different sites allows the structure to maintain a constant averaged X-site geometry in spite of the presence of a smaller cation at the X site ($^{[8]}$Sc = 0.87, $^{[8]}$Ca = 1.12 Å). This point will be discussed in detail in a forthcoming paper by our group (in preparation), which is focused on the site partitioning and local geometry of scandium in the garnet matrix.

The X1–O and X2–O values refined for sample 5 (2.344(1) and 2.497(1) Å, respectively) are slightly longer than in grossular and in samples 1 and 2, in keeping with the EXAFS results. We can conclude that the local Ca–O geometry is actually affected by the presence of larger cations at the octahedral (Fe^{3+}, with subordinate Fe^{2+} and Ti) and tetrahedral sites (H^{+}), as already suggested by comparison of the SREF data of grossular, andradite and hydrogrossular (cf. Fig. 6 and Ferro et al., 2003 and references therein).

EXAFS analysis of the Ca coordination in sample 3 (Ca = 1.20 apfu) and sample 4 (Ca = 0.51 apfu) gave a unique and almost constant Ca–O distance, namely 2.36 (1) and 2.35(1) Å, respectively. Hence, the coordination geometry is that of an almost regular 8-fold polyhedron, which results from a X1–O distance significantly longer and a X2–O distance far shorter than in grossular and in other compositions with Ca > 1.50 apfu. The X–O distances refined for the end-member pyrope synthesised by Ganguly et al. (1993) are 2.199(1) and 2.341(1) Å, respectively (again, $\Delta = 0.14$ Å). Hence, the individual X sites occupied by Ca in pyralspites are both smaller and more regular with respect to those in grossular, the unique Ca–O distance being as long as the longer Mg–O distance in pyrope. This change in coordination geometry is a suitable mechanism to host the larger Ca cation in the compact pyralspite structure. Actually, the averaged <X–O> distance (and thus the average site volume) obtained from EXAFS analysis for Ca in pyralspites (2.35 Å) is intermediate between that of calcium in the Ca-dominant samples (2.41 Å), and those of Mg in pyrope and of Fe^{2+} in almandine (2.27 and 2.30 Å, respectively).

It is well known that Mg is strongly dynamically disordered at the X site in pyrope (cf. Armbruster et al., 1992), the minimum X-site dimensions allowed by the garnet structure framework being too large for its coordination. The same situation, albeit in a far lesser extent, holds also for Fe^{2+} in almandine (Armbruster et al., 1992; Quartieri et al., 1997). The strong dynamic disorder (also called rattling) may be a reason for the lack of end-member pyrope in natural environments, where Fe^{2+} is almost ubiquitously present.

Quartieri et al. (1993) reported the EXAFS analysis at the Fe K-edge of some garnet compositions with Ca < 0.50 apfu (including sample 4 from this work) and of sample 5. The two-shell fits showed that the Fe coordination in this compositional range is always that of an irregular dodecahedron, with Fe1–O = 2.21–2.22 Å and Fe2–O = 2.37–2.41 Å. For comparison, the refined X1–O and X2–O distances in pure almandine are 2.223 and 2.374 Å, respectively. In the case of Fe^{2+} at the X site, the Δ values increase from 0.15 to 0.20 Å in the investigated compositional range. Unfortunately, EXAFS analysis of sample 5 allowed only an estimate of the Y–O distance for the dominant Fe^{3+} (2.00 Å). However, the homogeneity of the Fe^{2+} dodecahedral coordination geometry along the pyrope–grossular join is also supported by the observed constancy of Mössbauer isomer shifts (Amthauer et al., 1976).

No information is presently available for the local coordination of Mg along the join pyrope–grossular, and therefore XAS experiments at the Mg K-edge are planned by our group at the ELETTRA synchrotron radiation facility. Preliminary XANES results, obtained during a recent feasibility test, show slight variations along the series, suggesting only minor modifications of the Mg environment. However, a more accurate EXAFS analysis is necessary for a more precise description of the local environment of Mg in garnets. Based on the preliminary XANES

measurements and on the similarity in crystal-chemical behaviour with Fe^{2+}, it can be inferred that Mg should maintain a [4+4] coordination throughout the pyrope–grossular join, and that its Δ value should increase in pyralspites as a function of the grossular component. In this regard, it is also relevant to recall that EXAFS analysis at 77 K at the Yb L_I and L_{III} edges ($^{[8]}$Yb=0.98 Å) showed that the Yb^{3+}1–O and Yb^{3+}2–O distances are 2.25(2) and 2.33(2) Å (Δ=0.08 Å) in pyrope, but 2.24(2) and 2.38 (2) Å (Δ=0.14 Å) in grossular (Quartieri et al., 1999a).

4. Discussion

The results of this XAS study at the Ca K-edge can now be compared with those of previous work, and may explain the many anomalies observed. As discussed before, the Ca–O distances obtained here by multi-shell fits of EXAFS data allow interpretation of the differences in the XANES spectra. The bimodal behaviour (peaks labelled C and D in Fig. 2) in the spectra from samples with Ca>1.50 apfu, and the almost unimodal behaviour in pyralspites derives from the presence of two distinct local coordinations assumed by Ca in the two compositional ranges.

A comparison of EXAFS data with the long-range behaviour observed along the join is satisfactory in the case of sample 4, where a properly weighted combination of the available X1–O and X2–O values for the individual cations (obtained from EXAFS analysis for Fe and Ca, and from SREF for Mg in pyrope), yields X1–O=2.23 and X2–O=2.38 Å, in excellent agreement with the refined values (2.23 and 2.39 Å, respectively). In the case of sample 3, a weighted combination of the X1–O and X2–O distances estimated from EXAFS analysis at the Ca and Sc edges (for Sc, 2.18 and 2.32 Å, respectively; Quartieri et al., 2004a,b) with those refined for pyrope yields 2.26 and 2.35 Å respectively, to be compared with the refined values of 2.24 an 2.40 Å. It is thus clear that the longer X2–O distance cannot be modelled properly without considering a further distortion in the local coordination of Mg.

Comparative analysis of the refined atomic displacement parameters (adp) along the (prp, alm, sps)–grs join done at the CNR-IGG-PV shows that the adp of the O and T sites in the intermediate compositions are always strongly anisotropic, and much more so than those found in pyrope and grossular. The anisotropy is at a maximum around the $(prp, alm, sps)_{50}grs_{50}$ composition, where the major root mean square displacement of the O atom is 0.11 Å, to be compared with the values of the other two root-mean square components 0.06 and 0.07 Å (Boiocchi et al., 2000, and in preparation). Moreover, the adp at the O site has the major axis lying nearly along the X1–O bond (Fig. 7), a feature that could not be explained based on long-range analysis. This work shows that in pyralspites the individual X polyhedra occupied by Mg and Ca have quite similar X2–O distances (2.34 vs. 2.36 Å), but differ in their X1–O distances (2.20 vs. 2.36 Å). Hence, the observed anomalies in the adp at the O site, as well as their increase as a function of the Ca content in pyralspites, can now be explained in terms of differences in the local coordination of the individual O atoms. Interestingly, the shape of the adp at both the O and T sites becomes more regular at higher T values (CNR-IGG-PV, unpublished), suggesting a decrease in the static disorder, which may be interpreted, in the light of the present model, as a preferential lengthening of the X1–O distance. However, annealing of end-member pyrope and almandine produces a preferential increase of the atomic vibration along the X2–O distance (Armbruster et al., 1992; Quartieri et al., 1997; Sani et al., 2004). This difference is not trivial, because "the nature of the X-cation vibration affects garnet's thermodynamic properties" (Geiger, 2004).

Based on the results of this work, we can now tentatively provide an atomistic explanation for the asymmetry in the excess volume and enthalpy of mixing. As observed before, the volume of the almost regular dodecahedron occupied by Ca in the pyralspite structure is far smaller than that of the distorted dodecahedron occupied by Ca in the grossular structure. We have not yet been able to provide a model for local relaxation in the two different situations, but the size mismatching is smaller when the total amount of (Mg, Fe^{2+}, Mn^{2+}) is lower than 1.50 apfu.

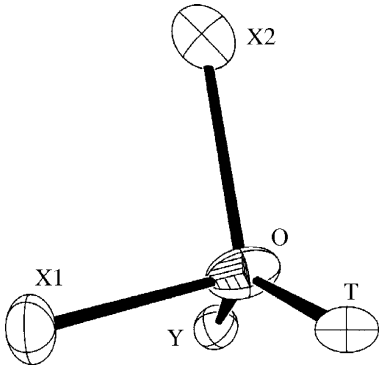

Fig. 7. ORTEP view of the local environment of the O site in a $Prp_{25}Alm_{25}Grs_{50}$ natural garnet (CNR-IGG-PV; unpublished). In this compositional range, the O ellipsoid is strongly elongated in the direction of the X1–O bond.

The above model is also consistent with the broadening (measured by Δ_{corr} analysis) of the spectral features commonly observed at the intermediate compositions, which is again indicative of the presence of a range of local distortions. All the spectroscopic works so far reported (cf. Geiger, 2004 for an exhaustive review) confirm that the prp–grs join is the most heterogeneous among garnets, and that heterogeneity is at the unit-cell scale. The presence of local heterogeneity implies the existence of strain gradients, and thus of local variations in the elastic energies. Boffa Ballaran et al. (1999) reported on the softening of low frequency IR modes at the intermediate prp–grs compositions, which might suggest some susceptibility towards a phase transition, which might in turn be associated with anomalies in local elastic properties.

The XAS analysis reported in this work shows that the local environments of Ca actually change around the (prp, alm, sps)$_{50}$grs$_{50}$ composition. The consequent structural rearrangement thus occurs at the instability point inferred from spectroscopic measurements; based on available information, this transition is isosymmetric.

A further important issue is the anomalous behaviour in relation to the incorporation of trace elements (e.g., REE and actinides) into the X site observed along the prp–grs join (cf. van Westrenen et al., 2003a, and references therein). In particular, the effective X-site modulus, E_X, calculated by elastic-strain modelling of experimental solid/melt partition coefficients is lower in the prp$_{60}$grs$_{40}$ composition than in both pyrope and grossular. This feature implies a greater compliance towards trace-element incorporation in the intermediate compositions, and again confirms a softening of the structure in this region.

Up to now, atomistic simulations of the prp–grs solid solution were done starting from discrete but analogous Mg and Ca sites, and converged to a model where Mg cations largely preserve the pyrope-type environment, and Ca cations predominantly preserve the grossular-type environment thorough the solid solution (Bosenick et al., 2000, 2001; van Westrenen et al., 2003a). They also showed that cation ordering in garnets is dominated by the third nearest-neighbour interaction between cations occupying two X dodecahedra, which share edges with the same tetrahedron. This interaction is more unfavourable for like cations (e.g., Mg–Mg), whereas Mg and Ca ordering in third-neighbour position minimises the strain in the connected tetrahedron. Based on these results, van Westrenen et al. (2003a) calculated solution energies for the various trace elements at different compositions, and found that for most dopants they are lower in prp$_{50}$grs$_{50}$ than in the end-members. These authors also stressed that Goldschmidt's first rule is not obeyed because, for instance, the solution energy for Ba in prp$_{50}$grs$_{50}$ is lower in a site occupied by Mg than in one occupied by Ca.

Further interpretative work is needed to resolve how the above model would change when two distinct local environments for Ca in the pyralspite-like and in the grossular-like structure were used. However, given the correlation between relaxation and defect energies, relatively large changes in defect thermodynamics are expected. From the structural point of view, we would suggest that the softening of the elastic modulus at the X site observed at the intermediate compositions by van Westrenen et al. (1999) might derive from the increasing instability of the structure when approaching the change in coordination geometry of the Ca cations.

Acknowledgements

This work benefited from the contribution of many persons, who are all warmly thanked for their help. Andrea Orlando (CNR-IGG, Firenze) prepared the starting materials for the synthesis of Sc-doped garnets; Detlef Krauße (Bayerisches Geoinstitut, Bayreuth) did their electron microprobe analysis. Funding for the project was provided by the MIUR-COFIN grant "Geo-crystal-chemistry of trace elements". **[LW]**

References

Allan, N.L., Du, Z., Lavrentiev, M.Yu., Blundy, J.D., Purton, J.D., van Vestrenen, W., 2003. Atomistic simulation of mineral–melt trace-element partitioning. Phys. Earth Planet., 93–111.

Amthauer, G., Annersten, H., Hafner, S.S., 1976. The Mössbauer spectrum of ^{57}Fe in silicate garnets. Z. Kristallogr 143, 14–55.

Ankudinov, A.L., Ravel, B., Rehr, J.J., Conradson, S.D., 1998. Real Space Multiple Scattering Calculation of XANES. Phys. Rev., B 58, 7565–7576.

Armbruster, Th., Geiger, C.A., Lager, G.A., 1992. Single-crystal X-ray structure study of synthetic pyrope–almandine garnets at 100 and 293 K. Am. Mineral. 77, 512–521.

Boffa Ballaran, T., Carpenter, M.A., Geiger, C.A., Koziol, A.M., 1999. Local structural heterogeneity in garnet solid solutions. Phys. Chem. Miner. 26, 554–569.

Boiocchi, M., Giannone, L., Prella, D., Oberti, R., 2000. The pyrope–grossular solid solution: new crystal-chemical data to model non-ideal behaviour. 3rd EMU workshop "Solid solutions in silicate and oxide systems of geological importance", Program, 7.

Bosenick, A., Dove, M.T., Geiger, C.A., 2000. Simulations studies of the pyrope–grossular solid solution. Phys. Chem. Miner. 27, 398–418.

Bosenick, A., Dove, M.T., Heine, V., Geiger, C.A., 2001. Scaling of thermodynamic mixing properties in garnet solid solutions. Phys. Chem. Miner. 28, 177–187.

Carboni, R., Giovanni, S., Antonioli, G., Boscherini, F., 2005. Self-absorption correction strategy for fluorescence-yield soft X-ray near edge spectra. Phys. Scr. T115, 986–988.

Ferro, O., Galli, E., Papp, G., Quartieri, S., Szakall, S., Vezzalini, G., 2003. A new occurrence of katoite and re-examination of the hydrogrossular group. Eur. J. Mineral. 15, 419–426.

Ganguly, J., Cheng, W., O'Neill, H.S.C., 1993. Syntheses, volume, and structural changes of garnets in the pyrope–grossular join: Implications for stability and mixing properties. Am. Mineral. 78, 583–593.

Geiger, C.A., 2004. Spectroscopic investigations relating to the structural, crystal-chemical and lattice-dynamic properties of $(Fe^{2+}$, Mn^{2+}, Mg, $Ca)_3Al_2Si_3O_{12}$ garnet: a review and analysis. In: Beran, A., Libowitzky, E. (Eds.), Spectroscopic Methods in Mineralogy. Eötvös University Press, Budapest, pp. 589–645.

Koninsberger, D.C., Prins, R. (Eds.), 1998. X-ray Absorption. Wiley and Sons, New York.

Larson, A.C., Von Dreele, R.B., 1997. GSAS: General Structure Analysis System. Document LAUR 86-748, Los Alamos National Laboratory.

Lee, P.A., Citrin, P.H., Eisenberger, P., Kincaid, B.M., 1981. Extended X-ray absorption fine structure—its strengths and limitations as structural tool. Rev. Mod. Phys. 53, 769–806.

Merli, M., Callegari, A., Cannillo, E., Caucia, F., Leona, M., Oberti, R., Ungaretti, L., 1995. Crystal-chemical complexity in natural garnets: structural constraints on chemical variability. Eur. J. Mineral. 7, 1239–1249.

Newville, M., 2001. IFEFFIT: interactive XAFS analysis and FEFF fitting. J. Synchrotron Radiat. 8, 322–324.

Pouchou, J.L., Pichoir, F., 1985. "PAP"$\varphi(\rho Z)$ procedure for improved quantitative microanalysis. In: Armstrong, J.T. (Ed.), Microbeam Analysis 1985. San Francisco Press, pp. 104–160.

Quartieri, S., Antonioli, G., Lottici, P.P., Artioli, G., 1993. X-ray absorption spectroscopy investigation at the Fe K-edge of natural garnets from Ivrea Verbano zone. Mineral. Mag. 57, 249–256.

Quartieri, S., Chaboy, J., Merli, M., Oberti, R., Ungaretti, L., 1995. Local structural environment of calcium in garnets: a combined structure-refinement and XANES investigation. Phys. Chem. Miner. 22, 159–169.

Quartieri, S., Antonioli, G., Artioli, G., Geiger, C.A., Lottici, P.P., 1997. A temperature dependent X-ray absorption fine structure study of dynamic X-site disorder in almandine: a comparison with diffraction data. Phys. Chem. Miner. 24, 200–205.

Quartieri, S., Antonioli, G., Geiger, C.A., Artioli, G., Lottici, P.P., 1999a. XAFS characterization of the structural site of Yb in synthetic pyrope and grossular garnets. Phys. Chem. Miner. 26, 251–256.

Quartieri, S., Chaboy, J., Antonioli, G., Geiger, C.A., 1999b. XAFS characterization of the structural site of Yb in synthetic pyrope and grossular garnets: II. XANES full multiple scattering calculations at the Yb LI- and LIII-edges. Phys. Chem. Miner. 27, 88–94.

Quartieri, S., Boscherini, F., Chaboy, J., Dalconi, M.C., Oberti, R., Zanetti, A., 2002. Characterization of trace Nd and Ce site preference and coordination in natural melanites: a combined X-ray diffraction and high-energy XAFS study. Phys. Chem. Miner. 29, 495–502.

Quartieri, S., Dalconi, M.C., Boscherini, F., Oberti, R., D'Acapito, F., 2004a. Crystal-chemistry of trace Rare Earth Elements in garnets by high-energy XAFS: new data on the site geometry of dysprosium. Phys. Chem. Miner. 31, 162–167.

Quartieri, S., Dalconi, M.C., Oberti, R., Boscherini, F., Iezzi, G., Boiocchi, M., 2004b. Site preference and partitioning of scandium in silicate garnets. 5° European Conference on Mineral Spectroscopy. Wien. Mitt. Osterr. Miner. Ges. 149, 82.

Quartieri, S., Dalconi, M.C., Oberti, R., Boscherini, F., Iezzi, G., Boiocchi, M., 2004c. Site preference and partitioning of scandium in silicatic garnets: first direct structural study. ESRF Experimental Report CH1545.

Sani, A., Quartieri, S., Boscherini, F., Antonioli, G., Feenstra, A., Geiger, C.A., 2004. Fe^{2+}–O and Mn^{2+}–O bonding and Fe^{2+}- and Mn^{2+}-vibrational properties in synthetic almandine–spessartine solid solutions: an X-ray absorption fine structure study. Eur. J. Mineral. 16, 801–808.

Sheldrick, G.M., 1996. SADABS. Siemens Area Detector Absorption Correction Program. University of Göttingen, Germany.

Toby, B.H., 2001. EXPGUI, a Graphical User Interface for GSAS. J. Appl. Crystallogr. 34, 210213.

Ungaretti, L., Leona, M., Merli, M., Oberti, R., 1995. Non-ideal solid solution in garnet: crystal-structure evidence and modelling. Eur. J. Mineral. 7, 1299–1312.

van Westrenen, Blundy, J.D., Wood, B.J., 1999. Crystal-chemical controls on trace-element partitioning between garnets and anhydrous silicate melts. Am. Mineral. 84, 838–847.

van Westrenen, W., Allan, N.L., Blundy, J.D., Lavrentiev, M.Yu., Lucas, B.R., Purton, J.A., 2003a. Trace element incorporation into pyrope–grossular solid solutions: an atomistic simulation study. Phys. Chem. Miner. 30, 217–229.

van Westrenen, W., Allan, N.L., Blundy, J.D., Lavrentiev, M.Yu., Lucas, B.R., Purton, J.A., 2003b. Dopant incorporation into garnet solid solutions—a breakdown of Goldschmidt's first rule. Chem. Commun., 786–787.

Vinograd, V.L., Slutter, M.H.F., Winkler, B., Putnis, A., Hålenius, U., Gale, J.D., Becker, U., 2004. Thermodynamics of mixing and ordering in pyrope–grossular solid solution. Mineral. Mag. 68, 101–121.